FROM COMPACTION TO FAILURE: CREEP ACCELERATION AND BUCKLE FORMATION IN A GLIDING SNOW BEAM

Grégoire Bobillier[1,2,*], Johan Gaume[2,3,4], Alec van Herwijnen[2], Christophe Ancey[1]

[1] *Environmental Hydraulics Laboratory, Ecole Polytechnique Federale de Lausanne, Lausanne, Switzerland*
[2] *WSL Institute for Snow and Avalanche Research SLF, Davos, Switzerland*
[3] *Climate Change, Extremes, and Natural Hazards in Alpine Regions Research Center CERC, Davos, Switzerland*
[4] *Institute for Geotechnical Engineering, ETH Zurich, Switzerland*

ABSTRACT: Glide-snow avalanches are difficult to predict and mitigate and can pose major challenges for the protection of roads, ski resorts, and buildings. They occur when the entire snow cover slowly slides downslope before suddenly releasing as an avalanche. The physical processes involved in the release of glide-snow avalanches remain poorly understood. To investigate snowpack deformation during gliding, we developed a laboratory tilt test under controlled cold-room conditions. A 1.67 m long snow beam rested on a temperature-controlled glass bed tilted at 30°; at the downslope end, an instrumented stop representing the mechanical support of a retention zone recorded the force, while the deformation of the beam side wall was monitored. Each test comprised a cold phase and a warm phase, during which the bed surface was heated above 0 °C to generate liquid water at the snow–glass interface. During the cold phase, most of the slope-parallel load was progressively transferred from the downslope stop to the basal interface. Within minutes of heating, this load returned to the stop and then remained nearly constant until failure. Under this constant load, deformation evolved from secondary to tertiary creep while the beam lost 55 % of its thickness, so that its density increased by a factor of about 2.5. Over the same interval the apparent compressive viscosity decreased by a factor of about 45, suggesting that viscous softening induced by the liquid water dominated the deformation response regardless the elastic stiffening expected from densification. Failure occurred abruptly within one buckle as the apparent strain rate approached 10^{-4} s^{-1}. These observations support a release scenario in which loss of basal resistance, progressive rheological softening and localized deformation lead to delayed failure without any increase in external loading. If similar rate-dependent behavior occurs at the slope scale, the temporal acceleration of surface deformation may provide a precursory signal for glide-snow avalanche forecasting.

KEYWORDS: Glide-snow avalanche release, tilt test, basal detachment.

1. INTRODUCTION

Glide-snow avalanches release the entire snowpack along the ground surface and involve large volumes of snow. Compared to other types of avalanches, glide-snow avalanches are considered difficult to predict and to mitigate, presenting a considerable challenge to protecting roads, railways, ski resorts, and buildings (e.g., Jones, 2004; Simenhois & Birkeland, 2010). Reliable glide-snow avalanche forecasting would reduce the cost of these closures and requires a solid understanding of the processes involved in their release.

On a slope, gravity induces normal and shear stresses in the snowpack, resulting in creep deformation. Under certain conditions, in addition to internal creep deformation, the entire snowpack may slowly slide along the ground, a mode of displacement referred as snow gliding (Ancey & Bain, 2015). Gliding is believed to result from a loss of friction along the snow-ground interface caused by the presence of liquid water and mainly occurs on smooth surfaces (McClung & Clarke, 1987; Newesely et al., 2000). As the snowpack moves, tensile stress develops and may produce a fracture through the entire depth of the snowpack (glide crack). Continued gliding can then lead to folding of the snowpack, to the formation of detached buckles and secondary cracks, and to increasing stresses at the downslope end until the compressed zone fails and the avalanche releases. Not every visual sign of snow gliding (glide crack, bulges and buckles) results in an avalanche. For those that do, the timing between these signs and the avalanche event can vary from hours to weeks, making predictions challenging. However, Fees, van Herwijnen, Altenbach, et al. (2025) have shown that most glide-snow avalanches release within 24 h after glide crack opening. Still, in their study, half of the glide- snow avalanches were released without a visible glide crack that could have served as a precursory signal.

During gliding, at the lower end of the snowpack, the snow decelerates and compacts against the retention zone (stauchwall).

** Corresponding author address:*
Grégoire Bobillier, WSL Institute for Snow and Avalanche Research SLF, Davos, Switzerland
email: gregoire.bobillier@slf.ch

https://doi.org/10.15788/1790098767

Haefeli (in Bader et al., 1939) described this compression zone and related its length l_c to snow depth, snow density through the creep angle, and the partition of the surface velocity between basal glide and internal deformation. Bucher (1948) and McClung (1982) describe how the deceleration of the snow against the obstacle reduces the basal shear resistance progressively and increase in the slope-parallel normal stress. Bartelt et al. (2012) recast this picture in terms of its time evolution: a local drop of the basal resistance redistributes stress towards the retention zone, which experiences a gradual increase in compressive stress, and the avalanche releases when the compressive strain rate exceeds a critical value. This model provides a compelling description of the release process, but, as Ancey and Bain (2015) point out, its quantification remains delicate and the retention zone is difficult to locate in the field, where it is usually destroyed by the avalanche itself.

Basal detachment and compressive failure are therefore both central in the accepted picture of glide-snow avalanche release, yet each has been deduced from field evidence and from model requirements rather than observed directly, and they have never been followed simultaneously on the same snowpack. How the snowpack deforms between the onset of gliding and the release, precisely the stage when visual signs appear, remains largely unknown.

We aim to describe the deformation of a snowpack gliding, on a substratum under dry and wet interfacial condition, from the onset of motion to snowpack failure. To this end, we developed a tilt test in a controlled environment (SLF cold laboratory), in which a 1.67 m long snow beam glides driven by gravitational loading is resting on a temperature-controlled glass bed. The configuration follows the sliding block experiments of Bader et al. (1939), who tested snow samples on an inclined glass plate, but the beam is here long enough for the deformation to localize, and its side wall is monitored so that the behavior of the interface itself becomes accessible. We measured the force applied at the downslope end of the beam, the deformation field along its side wall and the temperature at the snow-glass interface. We analyzed the thermo-mechanical response of the beam and the opening of the basal interface during one test performed at a slope angle of 30°.

2. DATA AND METHOD

2.1 Snow tilt test

To study snowpack deformation under controlled conditions, we adapted a tilt test inspired by soil mechanics (Figure 1). The setup extended the interface shear test of Bobillier et al. (2024) in three ways: the driving stress was provided by the slope-parallel component of gravity rather than by an externally applied force, the sample was long enough for the deformation to localize along the snow-glass interface, and the downslope end was retained by an instrumented stop representing the mechanical support provided by a natural retention zone.

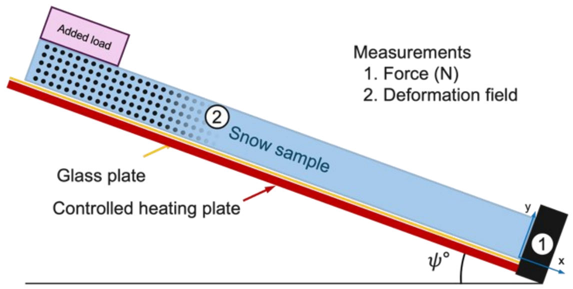

Figure 1: Experimental setup of the snow tilt test. A snow beam rests on a glass plate mounted on a temperature-controlled heating plate and inclined at a slope angle ψ. Two quantities were measured during each test: (1) the slope-parallel force F_s at the downslope stop, (2) the deformation field of the beam side wall, obtained by tracking the painted black pattern. The basal temperature T_b was recorded at the glass surface.

2.2 Experimental setup

The tests were performed in the SLF cold laboratory at a constant air temperature of −(1.5 ± 0.5) °C. The snow beam rested on a glass plate mounted on a temperature-controlled heating plate, both fixed to an aluminum frame that could be inclined at a slope angle ψ ranging from 0° to 45° (Figure 1). Glass was chosen as a smooth and impermeable bed, for which shear failure was previously shown to occur at the interface rather than within the snow (Bobillier et al., 2024). At the downslope end of the beam, a stop was instrumented with three 5 kg load cells recording the slope-parallel force F_s exerted by the gliding snow at 10 Hz. An additional load of 3.5 kg, equivalent to a 2 m extension of the beam, was applied on the surface at the upslope end of the beam and was required to initiate motion.

2.3 Sample preparation

The snow beam was sieved directly on the glass plate to a length of 1.67 m, a width of 25.5 cm and a height of 3 cm. We used snow that consist of decomposing and fragmented precipitation particles (DF) (Fierz et al., 2009), with an initial dry bulk density of 227 kg m^{-3}. The snow temperature was measured at $T_s \approx -1.5$ °C. Black paint was applied on one side wall of the beam to allow tracking of the deformed field, as commonly done in field tests (e.g, Propagation Saw Test, Bergfeld et al., 2021). After sieving, the beam was left to sinter for at least 30 min at $T_s \approx -1.5\,°C$ before tilting. After the sample preparation, the beam was tilted to the target angle chosen above friction angles (here, $\psi = 0$ to $30°$ in 4 min). Friction angles have been measured with a classic tilt test, $\phi_{dry} = 9.5°$ and $\phi_{wet} = 0.6°$.

2.4 Test procedure

Each test consisted of two successive phases. First a cold phase, the beam, the glass bed and the cold room were kept below freezing ($T_b \approx -1.5\,°\mathrm{C}, T_r \approx -1\,°\mathrm{C}$), so that no liquid water was present at the interface. Secondly a warm phase, the heating plate was raised to a controlled temperature above freezing ($T_b \approx 0.6\,°\mathrm{C}$) and the cold room was kept below freezing $T_r \approx -1\,°\mathrm{C}$, which generated liquid water at the snow-glass interface. The heating started after 162 min, and the test lasted 317 min

2.5 Deformation field measurement

One side wall of the beam was filmed throughout the test with a Fuji X-T2 camera recording one image every 1 sec. From side wall pictures, we computed two quantities. The global strain ε_g is the slope-parallel shortening of the beam normalized by its initial length. The beam thickness was measured at five positions along the side wall, away from the buckles, at the onset of heating and at the end of the test.

2.6 Basal detachment and buckle detection

The basal opening $g(x,t)$ was measured as the distance between the beam and the glass bed. We considered the interface locally detached when $g > 2$ mm, a threshold chosen above the measurement noise. We refer to a localized detached region accompanied by upward beam deflection as a buckle. Each buckle was labelled according to its position along the glass when first detected; for instance, B316 denotes a buckle initially detected at $\mathrm{x} = -316$ mm.

We conducted a series of five tests to assess the reproducibility of the observed thermo-mechanical response. All replicate tests showed the same overall sequence of rapid load transfer upon warming, creep acceleration under a nearly constant load, and abrupt localized failure.

3. RESULTS

Here, we present one test in detail performed at a slope angle $\psi = 30°$, which lasted 317 min and ended with the failure of the snow beam.

3.1 Deformation sequence

During the cold phase, a deformation of 0.4 % of the initial beam length was measured at the side wall (e.g. 7 mm, Figure 2a, b). At $t = 162$ min the heating was activated, $t = 172$ min the glass plate was at 0 °C starting the warm phase. At $t = 281$ min, that was 119 min after the onset of heating, the first buckle was detected 316 mm up to the downslope end of the beam (Figure 2.c). The buckle indicated that the snow had locally detached from the glass bed. Over the following 36 min, B_{316} grew and became clearly visible as a smooth buckle of the side wall (Figure 2.d). At $t = 309$ min, a second buckle (B_{535}) was detected and developed 219 mm upslope of the first one and was clearly visible at $t = 316$ min (Figure 2.f). One minute later, the buckle B_{535} failed. The strongly curved geometry of the buckle indicates that the local failure state combined axial compression and bending, although the local stress state could not be resolved directly from the present measurements. Immediately after, the upper part of the beam fragmented and slide downslope (Figure 2.f).

The beam also thinned markedly during the warm phase. Averaged over five positions away from the buckles, the thickness decreased from 29.3 mm at the onset of heating to 13.1 mm at the end of the test, a reduction of 55 %. Combined with the 9.2 % slope-parallel shortening, this corresponds to an estimated volume reduction of about 59 % in the strongly deforming part of the beam. The tangential force remained nearly constant over the same interval, which excludes a comparable loss of mass by meltwater drainage; the density of the beam therefore roughly doubled, to approximately 550 kg m^{-3}.

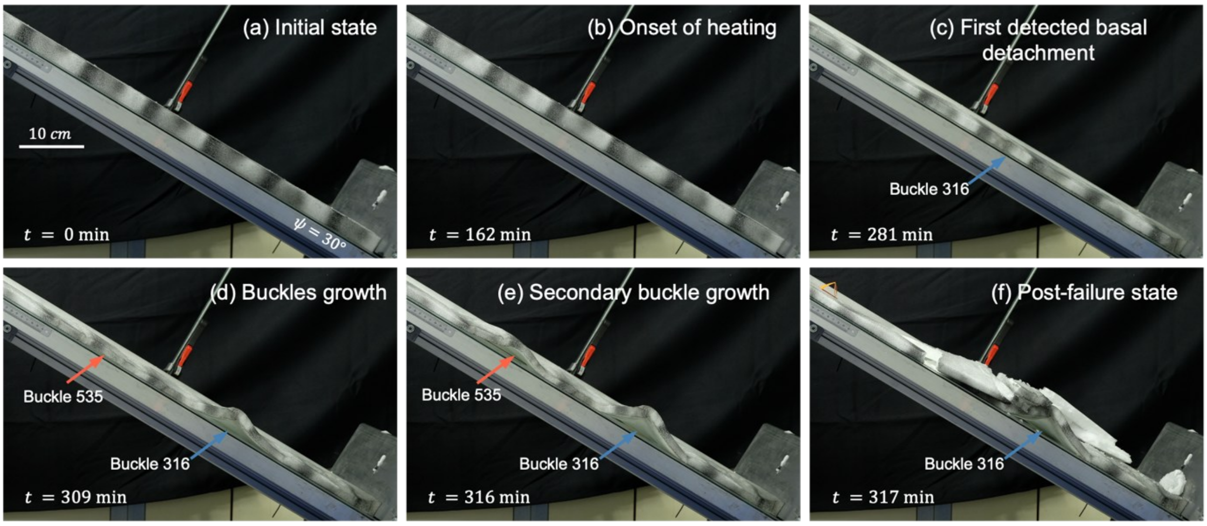

Figure 2: Side view of the snow beam during the tilt test at $\psi = 30°$. (a) Initial state after tilting. (b) Onset of bed-surface heating. (c) First detected buckle (buckle B_{316}). (d) Growth of B_{316}. (e) Growth of both buckles B535 and B_{316}. (f) State after failure of the beam (B_{535} failed)

3.2 Thermo-mechanical response

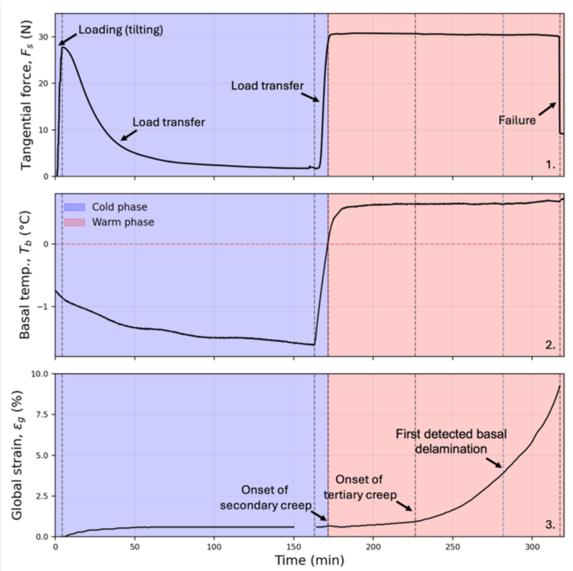

Figure 3: Thermo-mechanical response of the snow beam during the tilt test at $\psi = 30°$. (a) Tangential force F_s at the downslope stop, (b) basal temperature T_b, and (c) global strain ε_g as a function of time. The cold and warm phases are shaded in blue and red, respectively. The blue dashed line indicates the time of the first detected basal opening ($t = 281\ min$). The black dashed lines indicate process phases: (a) loading, (b) load transfer to interface, (c) load transfer to stop, (d) secondary creep, (e) tertiary creep until (f) failure.

Tilting the frame loaded the downslope stop and F_s increased to 27.7 N within 4 min (Figure 3.1). The slope-parallel component of the weight is shared between two supports: basal shear along the interface and the reaction force at the downslope stop, so that F_s measures the fraction of the driving load that the interface does not carry. Over the following 158 min, F_s decayed within approximately 60 min towards a plateau of 1.8 N, so that about 25.9 N were progressively taken up by basal shear, a mobilized ratio $\tau_b/\sigma_n \approx 0.54$, equivalent to a friction angle of 28.5°. The plateau was then maintained without measurable drift. This load transfer was accompanied by an initial global strain of 0.4 %, after which ε_g remained nearly constant (Figure 3.3). We interpret the initial 0.4 % strain as a compaction of the beam. During the cold phase, as the snow was colder than the room temperature, the basal temperature slowly decreased from −0.8 to −1.6 °C (Figure 3.2).

When the heating plate was switched on at $t = 162\ \mathrm{min}$, T_b passed above 0 °C within 9 min and then remained controlled at +0.6 °C until the end of the test (Figure 3.2). Over the same interval, the tangential force increased sharply from 1.8 to 30.8 N and subsequently remained nearly constant (Figure 3.1). This increase indicates that the slope-parallel load of the beam was transferred from the basal interface to the downslope stop as soon as liquid water was present at the interface. The beam deformed under a nearly constant load. We refer to the interval of approximately constant strain rate as secondary creep and to the subsequent interval of continuously accelerating strain rate as tertiary creep. During the secondary creep (Figure 3 phase (d)) (171 min to 226 min), the global strain increases from 0.4 % to 0.8 %. Starting $t = 226\ \mathrm{min}$ global strain accelerated continuously, reaching 9.2 % at the end of the test (Figure 3.3). This behavior is characteristic of tertiary creep (Figure 3, phase (e)). The first buckle was detected at $t = 281\ \mathrm{min}$, that is 55 min after the onset of tertiary creep. Thus, the acceleration of the beam preceded any detectable basal detachment. We define beam failure as the abrupt fracture of a buckle associated with a force drop and subsequent downslope motion of the upslope beam section. At $t = 317\,\mathrm{min}$, the force dropped abruptly from 30.8 to 9.1 N, as the beam failed.

4. DISCUSSION

The experiment reveals three main features of the deformation process. First, warming of the basal interface caused a rapid transfer of the snowpack load from bed surface to the downslope stop. Second, under this nearly constant load, deformation evolved from secondary creep to tertiary creep before localizing into discrete basal detachment. Third, the accelerating deformation culminated in abrupt failure within seconds, at strain rates consistent with a transition toward brittle behavior within a buckle. Together, these observations reveal a progression from load redistribution and distributed creep to localized deformation and rapid failure.

4.1 Load transfer

The load carried by the downslope stop changed twice during the test. At tilting, the stop carried almost the entire slope-parallel component of the weight. Over the following 158 min it decreased to 1.8 N, so that about 25.8 N were progressively taken up by basal shear resistance. As soon as the bed temperature raise above 0 °C, the load was rapidly transferred back to the downslope stop and remained nearly constant until failure. This abrupt response highlights the key role of interfacial liquid water in reducing basal resistance, consistent with field observations at Dorfberg, where soil temperature and liquid water content in the basal snow were identified as important controls on glide-snow avalanche occurrence (Fees, Van Herwijnen, Lombardo, et al., 2025). The basal interface had lost essentially most of its resistance, and the load was transferred back to the stop within minutes. This is the sequence that underlies the accepted picture of glide-snow avalanche release, in which the loss of friction at the snow-ground interface redistributes stress towards the retention zone at the lower end of the gliding slab, which may eventually fail (Bartelt et al., 2012; McClung & Clarke, 1987). In our setup, the instrumented stop represents the mechanical support provided by a retention zone, the measured force provides a direct estimate of the load and loading history that such a zone must sustain.

4.2 Delayed buckle formation

Localized deformation occurred late: the acceleration of deformation preceded the first detectable basal detachment by 55 min and developed while the beam remained apparently attached to the bed. Failure then occurred in the buckle that was growing fastest at the end of the test rather than in the one that had reached the largest opening, consistent with a rate-controlled transition.

4.3 Viscous softening under a constant load

Once the interface was wet, the force at the stop reached 98% of the slope-parallel component of the weight, so that the residual basal shear was negligible. Under this nearly constant load, an apparent compressive viscosity was estimated as $\eta = \bar{\sigma}_c/\dot{\varepsilon}_g$, where $\bar{\sigma}_c$ is the axial compressive stress averaged along the beam. From secondary creep to the end of the test, the strain rate increased by approximately two orders of magnitude, while the apparent compressive viscosity decreased by a factor of about 45. This reduction occurred despite a density increase by a factor of approximately 2.5, indicating that the softening induced by warming and the presence of liquid water surpassed the stiffening associated with densification and led to progressive viscous softening of the snow. Although this apparent viscosity is not equivalent to the Maxwell viscosity, its evolution is qualitatively consistent with the importance attributed to snow viscosity in the model introduced by Bartelt et al. (2012).

At failure, the apparent compressive strain rate reached approximately $10^{-4}\,s^{-1}$. This is of the same order as the ductile-to-brittle transition reported by Narita (1980) for snow in uniaxial tension and the shear strain rate at which Puzrin et al. (2019) identify a transition from rate-hardening to rate-softening. It is, however, about two orders of magnitude below the critical compressive strain rate of approximately $10^{-2}\,s^{-1}$ adopted by Bartelt et al. (2012) from triaxial tests (Scapozza & Bartelt, 2003) as a failure criterion for the retention zone. These comparisons involve different loading modes and should therefore be regarded as indicative rather than as evidence for a universal critical strain rate.

4.4 Limitations

Several limitations should be kept in mind. The glass bed is smooth and impermeable and therefore reproduces neither the roughness of a natural ground nor the water exchange across the snow-soil interface. The normal stress at the interface, about 130 Pa, is a factor of a few lower than under a shallow gliding snowpack of 10 to 40 cm. The beam is also short compared to a real slope, and the upslope load and the downslope stop are idealized boundary conditions. These differences limit the direct quantitative transfer to the slope scale.

5. CONCLUSION

We developed a laboratory tilt test under controlled cold chamber conditions. This test allowed us to track the deformation of a sliding snow beam, from compaction to failure, while simultaneously measuring the basal opening and the load transferred to a downslope support playing the role of a retention zone. Warming of the basal interface above 0 °C and the resulting formation of liquid water triggered gliding, causing a rapid loss of basal resistance and transferring most of the driving load to the downslope support. The beam subsequently evolved from secondary to tertiary creep under a nearly constant load.

During tertiary creep, the apparent compressive viscosity decreased by a factor of approximately 45 regardless of strong densification, indicating progressive rheological softening. The acceleration of deformation preceded the first detectable buckle by 55 min, showing that deformation localization was a late-stage manifestation of an instability that initially developed as distributed deformation. Failure finally occurred abruptly within a strongly deformed buckle as the apparent strain rate approached (10^{-4} s^{-1}), consistent with a transition toward brittle behavior.

These observations support a picture of glide-snow avalanche release in which loss of basal resistance, progressive rheological softening, and localized deformation can lead to delayed failure without an increase in external loading. If similar rate-dependent behavior occurs at the slope scale, the temporal acceleration of surface deformation could provide a useful precursory signal for glide-snow avalanche forecasting.

6. REFERENCES

Ancey, C., & Bain, V. (2015). Dynamics of glide avalanches and snow gliding. *Reviews of Geophysics*, *53*(3), 745-784. https://doi.org/10.1002/2015rg000491

Bader, H., Haefeli, R., Bucher, E., Neher, J., Eckel, O., & Thams, C. (1939). *Der Schnee und seine Metamorphose*. Kümmerly and Frey.

Bartelt, P., Feistl, T., Bühler, Y., & Buser, O. (2012). Overcoming the stauchwall: Viscoelastic stress redistribution and the start of full-depth gliding snow avalanches. *Geophysical Research Letters*, *39*, L16501, Article L16501. https://doi.org/10.1029/2012gl052479

Bergfeld, B., van Herwijnen, A., Reuter, B., Bobillier, G., Dual, J., & Schweizer, J. (2021). Dynamic crack propagation in weak snowpack layers: insights from high-resolution, high-speed photography. *The Cryosphere*, *15*(7), 3539-3553. https://doi.org/10.5194/tc-15-3539-2021

Bobillier, G., Fees, A., Lombardo, M., Schöttner, J., Cabrera, M., van Herwijnen, A., Gaume, J., & Schweizer, J. (2024). Towards an improved understanding of glide-snow avalanche release: interface shear cold laboratory tests. Proceedings ISSW 2024. International Snow Science Workshop, Tromso, Norway, 23-27 September 2024,

Bucher, E. (1948). Beitrag zu den theoretischen Grundlagen des Lawinenverbaus. *Kommissionsverlag Kümmerli & Frey, Bern*, 113.

Fees, A., van Herwijnen, A., Altenbach, M., Lombardo, M., & Schweizer, J. (2025). Glide-snow avalanche characteristics at different time scales extracted from time-lapse photography. *Annals of Glaciology*, *65*, e3. https://doi.org/10.1017/aog.2023.37

Fees, A., Van Herwijnen, A., Lombardo, M., & Schweizer, J. (2025). Towards a model of glide-snow avalanche occurrence using in-situ soil and snow measurements. *Journal of Glaciology*, *71*, e119.

Fierz, C., Armstrong, R. L., Durand , Y., Etchevers, P., Greene, E., McClung, D. M., Nishimura, K., Satyawali, P. K., & Sokratov, S. A. (2009). *The International Classification for Seasonal Snow on the Ground* (Vol. 83). UNESCO-IHP.

Jones, A. (2004). Review of glide processes and glide avalanche release. *Avalanche News*, *69*, 53-60.

McClung, D. M. (1982). A one-dimensional analytical model for snow creep pressure on rigid structures. *Canadian Geotechnical Journal*, *19*, 401-412.

McClung, D. M., & Clarke, G. K. C. (1987). The effects of free water on snow gliding. *Journal of Geophysical Research*, *92*(B7), 6301-6309.

Narita, H. (1980). Mechanical behaviour and structure of snow under uniaxial tensile stress. *Journal of Glaciology*, *26*(94), 275-282.

Newesely, C., Tasser, E., Spadinger, P., & Cernusca, A. (2000). Effects of land-use changes on snow gliding processes in alpine ecosystems. *Basic and Applied Ecology*, *1*(1), 61-67. https://doi.org/10.1078/1439-1791-00009

Puzrin, A. M., Faug, T., & Einav, I. (2019). The mechanism of delayed release in earthquake-induced avalanches. *Proceedings. Mathematical, physical, and engineering sciences*, *475*(2227), 20190092.

Scapozza, C., & Bartelt, P. (2003). Triaxial tests on snow at low strain rate. Part II. Constitutive behaviour. *Journal of Glaciology*, *49*(164), 91-101. <Go to ISI>://000188771100010

Simenhois, R., & Birkeland, K. (2010). Meteorological and environmental observations from three glide avalanche cycles and the resulting hazard management technique. Proceedings ISSW 2010. International Snow Science Workshop, Lake Tahoe CA, U.S.A., 17-22 October 2010,